Publication Year	2023
Acceptance in OA	2025-03-14T17:46:21Z
Title	The Io, Europa, and Ganymede Auroral Footprints at Jupiter in the Ultraviolet: Positions and Equatorial Lead Angles
Authors	Hue, V., Gladstone, G. R., Louis, C. K., Greathouse, T. K., Bonfond, B., Szalay, J. R., Moirano, A., Giles, R. S., Kammer, J. A., Imai, M., MURA, Alessandro, Versteeg, M. H., Clark, G., Gérard, J.-C., Grodent, D. C., Rabia, J., Sulaiman, A. H., Bolton, S. J., Connerney, J. E. P.
Publisher's version (DOI)	10.1029/2023JA031363
Handle	http://hdl.handle.net/20.500.12386/36830
Journal	JOURNAL OF GEOPHYSICAL RESEARCH. SPACE PHYSICS
Volume	128

The Io, Europa and Ganymede auroral footprints at Jupiter in the ultraviolet: positions and equatorial lead angles

V. Hue[1*], G. R. Gladstone[1,2], C. K. Louis[3], T. K. Greathouse[1], B. Bonfond[4], R. S. Giles[1], J. A. Kammer[1], M. Imai[5], A. Moirano[6], A. Mura[6], M. H. Versteeg[1], G. Clark[7], J.-C. Gérard[4], D. C. Grodent[4], A. Sulaiman[8], J. R. Szalay[9], S. J. Bolton[1], J.E.P. Connerney[10,11]

[1]Southwest Research Institute, San Antonio, Texas, USA
[2]University of Texas at San Antonio, San Antonio, Texas, USA
[3]School of Cosmic Physics, DIAS Dunsink Observatory, Dublin Institute for Advanced Studies, Dublin, Ireland
[4]STAR Institute, LPAP, Université de Liège, Liège, Belgium
[5]Department of Electrical Engineering and Information Science, National Institute of Technology (KOSEN), Niihama College, Niihama, Japan
[6]Institute for Space Astrophysics and Planetology, National Institute for Astrophysics, Rome, Italy
[7]Johns Hopkins University Applied Physics Laboratory, Laurel, MD, USA
[8]Minnesota Institute for Astrophysics, School of Physics and Astronomy, University of Minnesota, Minneapolis, MN, United States
[9]Department of Astrophysical Sciences, Princeton University, Princeton, NJ, USA
[10]NASA Goddard Spaceflight Center, Greenbelt, MD 20771, USA
[11]Space Research Corporation, Annapolis, MD 21403, USA

Key Points:

- Over 1600 ultraviolet spectral images of the Io, Europa and Ganymede footprints from Juno are analyzed
- Empirical formulae for the Io, Europa and Ganymede lead angles derived from Juno data are provided
- Including the equatorial lead angle in modeling the moon-induced decametric emission significantly improves the electron energy determination

---

*vhue@swri.edu

Corresponding author: V. Hue, `vhue@swri.org`

Abstract

Jupiter's satellite auroral footprints are a consequence of the interaction between the co-rotating iogenic plasma and the Galilean moons. The created disturbances near the moons propagate as Alfvén waves along the magnetic field lines. The physical positions of the moons are therefore magnetically connected to their respective footprint. As a result of the moon-magnetosphere interaction, decametric radio emission are emitted around the magnetic field line connected to the satellite footprints and narrowly spatially beamed. Interpretation of the moon-induced decametric emission depends on the time for the Alfvén waves to travel from the interaction region near the moons to Jupiter's ionosphere, also known as the "equatorial lead angle". Using spectral images recording by Juno of the Main Alfvén Wing auroral spots collected during the first forty-third orbits, this work provides an empirical model of the Io, Europa and Ganymede equatorial lead angles for the northern and southern hemispheres. Additionally, this work demonstrate the accuracy of the magnetic mapping from the Juno reference model at the completion of the prime mission for M-shells going at least to $15\,\mathrm{R}_J$.

Plain Language Summary

The interaction between the Jovian magnetodisk and the Galilean moons involves a complex set of observable phenomenon, including the generation of auroral spots magnetically connected to the moons and the generation of decametric emissions. Studying the position of these auroral spots and how they vary over a complete Jovian rotation provides information about the magnetic mapping, as they map directly to the actual physical position of the moons. The present work extends the earlier surveys provided by the Hubble Space Telescope. The magnetic field model derived from Juno's prime mission is in very good agreement with the observation of the satellite footprints. The position of the auroral spot also informs on how the electromagnetic perturbation resulting from the interaction propagates to creates the auroral spots, also known as the "equatorial lead angle". That latter information is particularly important to interpret moon-induced decametric radio emission, an emission narrowly beamed around the magnetic field lines connected to each auroral spots. The present work provides an empirical fit of the equatorial lead angle for Io, Europa and Ganymede derived from Juno data.

1 Introduction

Jupiter's volcanically-active moon Io is a major source of plasma in the jovian magnetosphere. About one ton of sulfur dioxide escapes from the moon per second as a neutral cloud around the moon. High energy electrons trapped in Jupiter's magnetosphere dissociate and ionize the neutral material, which gets picked up by Jupiter's strong magnetic field, forming the Io plasma torus. The plasma is then radially transported outwards over the timescale of several weeks as a plasma sheet several Jupiter's radii-thick ($1\ \mathrm{R}_J = 71492\,\mathrm{km}$), and confined in the centrifugal equator, near the magnetic equator (e.g., Thomas et al., 2004).

The Galilean moons act as obstacle to the corotating plasma, generating plasma and magnetic field perturbation that propagates as Alfvén waves along Jupiter's magnetic field lines, both ways towards the northern and southern jovian ionosphere. When the Alfvénic perturbations reach high Jovian latitudes, they accelerate electrons towards and away from Jupiter, leading to the generation of the auroral footprints and decametric radio waves (e.g., Bagenal & Dols, 2020). The radio waves resulting from the magnetospheric interaction at Io was discovered early on by Bigg (1964), later followed by the detection of the associated infrared (IR) and ultraviolet (UV) auroral footprint Connerney et al. (1993); Clarke et al. (1996). Compared to Europa and Ganymede, the moon-magnetosphere interaction is amplified at Io because of the stronger background Jovian magnetic field.

Detection of the Europa and Ganymede auroral footprints using the Hubble Space Telescope (HST) followed shortly after (Clarke et al., 2002).

Because Jupiter's magnetic dipole is tilted from its rotation axis, the plasma sheet sweeps through the Galilean moons twice every $\sim$10 hour-rotation period. In the reference frame attached to the plasma sheet, the moons travel up and down the sheet, experiencing denser plasma condition at the center of the sheet. Extensive HST campaigns over the last two decades revealed that the morphology of the Io footprints are controlled by the position of the moon in the plasma sheet, or centrifugal latitude (Gérard et al., 2006; Bonfond et al., 2008). Alfvén waves are partially transmitted and reflected on the plasma density gradients such as the plasma sheet boundary and the Jovian ionosphere, bouncing between Jovian hemispheres (Neubauer, 1980; S. L. G. Hess, Delamere, et al., 2010). This creates complex patterns of auroral footprints modulated by the moon centrifugal latitude. The idea of bouncing Alfvén waves was initialling proposed by Gurnett and Goertz (1981) as the processes responsible for the observation of the multiple Io-controlled decametric radio arcs.

Extensive HST campaigns have allowed classifying the variable morphology of the Io footprint structure as a function of the located of Io with respect to the plasma sheet (Gérard et al., 2006; Bonfond et al., 2008). These studies showed that the main Alfvén wing (MAW) spot was preceded by another spot, named the Transhemispheric Electron Beam (TEB), for a very specific range of sub-Io Jovian longitudes. In that case, the Alfvén waves generated in the wing of the interaction region arrived later at Jupiter's ionosphere, meaning the beam of electron generating the TEB spot was accelerated anti-planetward by the MAW on the opposite hemisphere, then travelled across the magnetic field line throughout the torus, unaffected by the higher torus plasma density (Bonfond et al., 2008).

The Juno mission has brought a wealth of new observations that significantly furthered our understanding of the moon-magnetosphere interaction (Bolton et al., 2017; Connerney et al., 2017). Juno crosses at least twice per orbit the fluxtubes connecting the Galilean moons, or connected to the interaction region downstream of the plasma flow, with the different parts of the footprint tail structure. Not only Juno measured the field and particles within the magnetic fluxtube connected to the discrete auroral footprint spots or tail, but it also provided unprecedented infrared and ultraviolet observations either at the highest spatial ever achieved (Mura et al., 2018), or with observation geometries not accessible from HST (Hue, Greathouse, et al., 2019).

Early Juno measurements demonstrated the Alfvénic nature of the interaction generating the Io footprint tail (Szalay et al., 2018; Damiano et al., 2019; Gershman et al., 2019; Sulaiman et al., 2020), settling the debate about the processes responsible for the footprint tail generation (e.g., Bonfond, Saur, et al., 2017; Delamere et al., 2003). Juno demonstrated that the electron energy flux responsible for the tail emission decreases exponentially downstream of the interaction region, and was best organized with the angle along Io's orbit between Io and an Alfvén wave trajectory connected to the aurora, also coined "Io-Alfvén tail distance" (Szalay et al., 2020b). Juno measured upward ion conics-protons with angular distribution concentrated along the loss-cone-detected simultaneously with ion cyclotron waves, and showing that energetic ions are also generated from moon-magnetosphere interaction (Clark et al., 2020). Additionally, the cyclotron maser instability (CMI) driven by loss-cone distribution function has been established as a major process at Jupiter in generating hectometric and decametric emissions, induced or not by the Galilean moons (Louarn et al., 2017, 2018; Louis et al., 2020).

Alfvénic acceleration processes was also witnessed when crossing the fluxtube connected to Ganymede's footprint tail (Szalay et al., 2020a). One particular Ganymede fluxtube crossing, during which Juno was connected to the leading-most Ganymede auroral spot for the first time, brought a set of in-situ and remote sensing measurements consistent with what was expected during a TEB crossing (Hue et al., 2022). Unlike for Io and Ganymede, crossing through the fluxtube connected to the Europa footprint tail showed signs of electron distribution resulting at least in part from electrostatic acceleration processes (Allegrini et al., 2020a). Whether this is a fundamental difference of the interaction at Europa remains to be proven with studies on additional Europa footprint tail crossings.

The scope of this paper is to process the ultraviolet auroral footprint observations performed from the first perijove (PJ, herefore) on 8 Aug 2016 until PJ43 (5 Jul 2022) by the ultraviolet spectrograph on Juno (Juno-UVS). First is described the observations and data reduction procedure. Second, the reported satellite footprint locations are compared against the predicted satellite footpaths from the magnetic field model JRM33 (Connerney et al., 2022). We then calculate the equatorial lead angles for Io, Europa and Ganymede and provide an empirical fit. Finally, we apply the knowledge of the lead angle to the interpretation of the Ganymede-induced decametric emission.

2 Juno-UVS observations

Juno is a spin-stabilized spacecraft placed on a polar and elliptical orbit around Jupiter since July 2016 (Bolton et al., 2017). Every orbit, Juno performs a close flyby of the northern polar region first, reaches closest approach at lower jovian latitudes with a closest approach altitude of about 4000 km, and then flies above the southern polar region. Because Juno's orbit is highly elliptical and because its closest approach velocity with respect to Jupiter is about 58 km/s, it takes Juno about 2 hours to fly from north to south pole. This implies the spatial resolution of the remote sensing instrument such as UVS to varies drastically over the course of a perijove observation sequence. As the mission goes, the orbital period, which initially started around 43 days, was reduced into a shorter orbit, and will be reduced down to 33 days around PJ75 (15 Aug 2025). Each major orbital period reduction follows a Galilean moon flybys. Juno's orbit precesses as a function of time, with the sub-spacecraft PJ latitude increasing north as the mission goes. The viewing window of UVS over the northern and southern auroras grows increasingly more asymmetric with the mission, with the viewing time of the northern aurora decreasing over time.

Some of the magnetospheric goals of Juno include performing in-situ measurements of the particle population in Jupiter's magnetosphere using an electron and ion sensors suite, while remotely sensing the associated infrared and ultraviolet aurora they may trigger on Jupiter or on the Galilean moons (Bagenal et al., 2017). The Ultraviolet Spectrograph (UVS) is a photon-counting imaging spectrograph operating in the 68-210 nm range (Gladstone et al., 2017). Each spin of Juno, UVS records a swath of UV emission along its 7.2°-long slit, with a typical point-source integration time of 17 ms. The point-spread function (PSF) and spectral resolution are respectively 0.1° and 1.3 nm, at best (Davis et al., 2011; Greathouse et al., 2013). Counts recorded on the detector are then converted into brightness using the instrument effective area derived from thousands of stellar observations recorded throughout the mission in between PJ observation sequences (Hue, Gladstone, et al., 2019; Hue et al., 2021).

UVS possesses a scan mirror that allows its field of regard to be shifted up to ±30° away from the spin plane. Juno's spinning nature combined with UVS' mirror pointing capability allows building up complete maps of Jupiter's aurora by co-adding consecutive swaths of data. The best temporal resolution of UVS is constrained by the spin rate of Juno and cannot be less than 30 seconds.

The satellite auroral footprints represent a direct mapping of the magnetic field of the Galilean moons, through the prism of the sub-Alfvénic interaction around each moon. Because of the Jovian rotation and the moon orbital motion, there is a longitudinal displacement of the satellite footprints between two consecutive UVS images recorded 30 seconds apart, which can be estimated considering each moon's synodic period:

$$P^{syn}_{moon} = \frac{P_J\, P_{moon}}{P_{moon} - P_J}, \qquad (1)$$

where P$_J$ and P$_{moon}$ are respectively the rotation period of Jupiter and orbital periods of a moon. Relationship (1) leads to P$^{syn}_{io}$ = 12.89 h; P$^{syn}_{europa}$ = 11.22 h; P$^{syn}_{ganymede}$ = 10.53 h. Over the course of a Juno spin (∼30 seconds), the longitudinal displacement of the moon is $\Delta\lambda_{moon} = 360 \times 30/P^{syn}_{moon}$, where P^{syn}_{moon} is in seconds. This leads to $\Delta\lambda_{io} = 0.23°$; $\Delta\lambda_{europa} = 0.27°$; $\Delta\lambda_{ganymede} = 0.28°$. Over one Juno spin and using the JRM33 model, this leads to a displacement of the instantaneous field line from the moon to Jupiter's northern ionosphere of 66-223 km, 67-220 km, 58-191 km, respectively for Io, Europa and Ganymede. In the south, that same smearing ranges 73-141 km, 76-136 km, 65-114 km for Io, Europa and Ganymede. Note that all longitudes (λ) quoted in this work are W-longitudes in the System III.

In order to increase the signal to noise ratio (SNR), while limiting the smearing the satellite footprint, the choice was made to bin the UVS data by 2 consecutive spins worth of data. A procedure was written designed to extract the precise location of the multiples auroral footprints of Io, Europa and Ganymede. In many cases, various auroral emissions may be present close to the footprint, such as increased auroral oval emission (Bonfond et al., 2021; Ebert et al., 2021), injection signatures (e.g., Bonfond, Gladstone, et al., 2017), or increased background radiation (Bonfond et al., 2018; Kammer et al., 2019). The change of geometry, background emission and SNR makes extracting automatically the precise location of the footprints challenging, particularly for the Europa and Ganymede footprints, generally located rather close from main oval emission and auroral injection. The footprint locations were manually extracted by visual inspection of consecutive series of 2 spins-averaged UVS data. Since the moons are not in co-rotation with Jupiter, identifying the satellite footprints over consecutive spins worth of data is achieved by visually inspecting auroral spots that are in sub-corotation around a background of mostly corotating auroral emission. Figure 1 shows an example of consecutive 2-spin averaged spectral image recorded by UVS of the Io, Europa and Ganymede footprints.

The uncertainties on the derived location of the different footprints were calculated as the quadratic combination of the uncertainty due to the instrument point-spread-function (PSF), and the uncertainty due to the projected scale height H of the footprint emission curtain. While the former uncertainty only depends on the distance between Juno and the considered footprint, the latter depends on the footprint emission angle as seen by Juno. The uncertainties on the footprint longitude (λ), latitude (ϕ) therefore reads:

$$\sigma^2_{\lambda,\phi} = \sigma^2_{PSF} + {\sigma_P}^2_{\lambda,\phi}, \qquad (2)$$

where σ_{PSF} is calculated as the projection of the $\sim$ 0.1° UVS PSF along the altitude and longitude grid. $\sigma_{P\lambda,\phi}$ is calculated from the projection vertical extent of the footprint emission curtain, H, as illustrated on Fig. 2. P is given as P = H/tan β, and $\beta = \pi/2$ - e - ϵ, where e and ϵ are calculated using NAIF's SPICE kernels (C. H. Acton, 1996; C. Acton et al., 2018). H was taken 366 km, *i.e.,* the typical scale height of a Chapman profile derived from Io's MAW spot by Bonfond (2010).

Only the data recorded by UVS when Juno was ± 1.5 hours about perijove was used, *i.e.,* when the $\sim$ 0.1° PSF projected at 45° on Jupiter's surface is lower than typical width of the footprint as previously derived from HST. From PJ1 until PJ43, this results in a set of 2-spin averaged UVS images of 211, 108 and 160 in the north, and 585, 264 and 299 in the south, respectively for Io, Europa and Ganymede. The projection al-

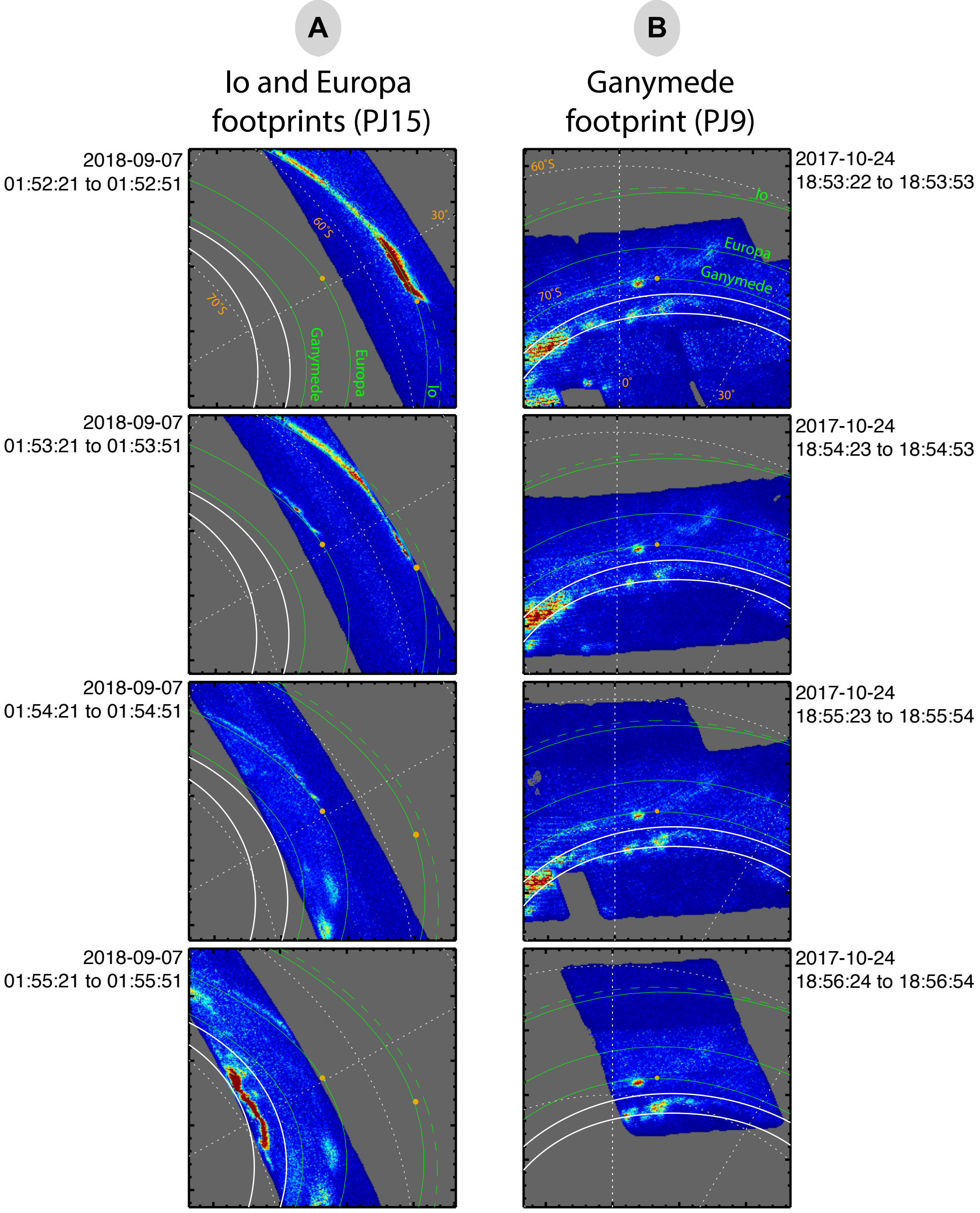

Io and Europa footprints (PJ15)

Ganymede footprint (PJ9)

2018-09-07
01:52:21 to 01:52:51

2018-09-07
01:53:21 to 01:53:51

2018-09-07
01:54:21 to 01:54:51

2018-09-07
01:55:21 to 01:55:51

2017-10-24
18:53:22 to 18:53:53

2017-10-24
18:54:23 to 18:54:53

2017-10-24
18:55:23 to 18:55:54

2017-10-24
18:56:24 to 18:56:54

Figure 1. 2-spin averaged Juno-UVS spectral images of the Io and Europa footprint (panel A), and the Ganymede footprint (panel B) over the southern hemisphere. The UVS nadir time of the two consecutive spins are listed as UTC time. The instantaneous moon magnetic position according to the JRM33 model is shown as orange dots along the satellite footprints, also calculated using JRM33 and shown as solid green line. The satellite footpath of Io from Bonfond, Gladstone, et al. (2017) is shown as dashed green lines. The solid white lines show the reference oval from Bonfond et al. (2012).

titude of the UV data on Jupiter used for this work was 900 km above the 1-bar level, after Bonfond (2010); Szalay et al. (2018).

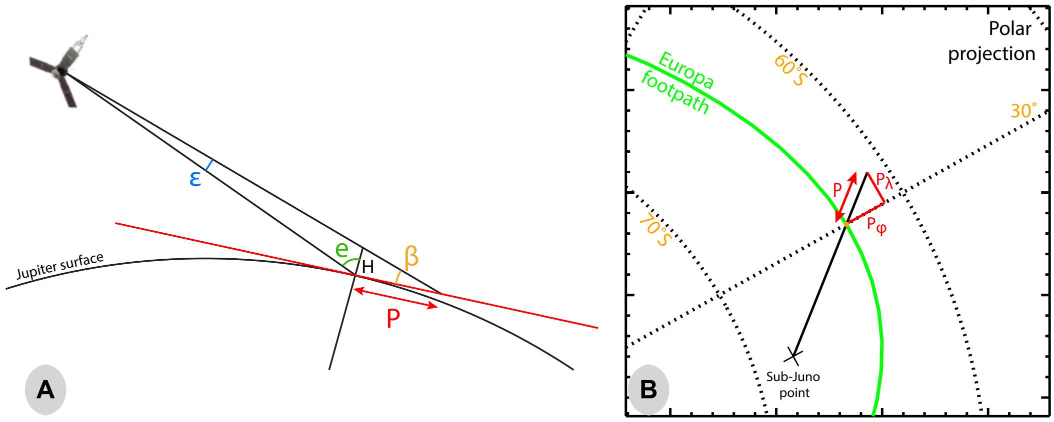

Figure 2. Uncertainty calculation on the derived latitude and longitude of the footprints. Panel A: calculation of the projected height the auroral footprint curtain P along the Juno line of sight. The latitude and longitude uncertainty (P_ϕ, P_λ) are calculated through the decomposition of P, exaggerated here for illustration purposes, along the latitude and longitude grid (panel B).

3 Satellite footprint location

Measuring the precise location of the satellite footprints provides a precise magnetic mapping of actual position of the moons. Several earlier magnetic field models of Jupiter were constructed using in-situ spacecraft measurements as well as the Io footprint location derived from IR and UV observations. This initially allowed Connerney et al. (1998) to build the VIP4 model, using observations of the Io footprint in the IR. Using a larger set of Io footprint observations obtained in the UV, the method was extended by S. L. G. Hess et al. (2011) to produce the VIPAL magnetic field model. That later model additionally included the longitudinal constraint on the Io footprint location, which originates from the finite Alfvén travel time between the interaction region near the moon and Jupiter's ionosphere.

The position of the Io, Europa and Ganymede footprints are presented on Fig. 3, and are plotted against the satellite footpath contours predicted from the JRM33 model (Connerney et al., 2022). Unlike the HST observations, UVS observed the footprints with a wide range of emission angle, from 1° to 77°, as well as a wide range of altitude, from $0.3\,\mathrm{R}_J$ to $2.6\,\mathrm{R}_J$ (where $1\,\mathrm{R}_J = 71492\,\mathrm{km}$)

Because of the precession of Juno's orbit, Juno-UVS gets an increasingly shorter look over the northern aurora as the mission progresses. This causes a greater density of footprint position measurements in the south, despite the rapid increase of Juno's altitude over the south pole during outbound. The magnetic field model obtained after the completion of the prime mission predicts a magnetic footpath for the satellite in very good agreement with the Juno-UVS observations (Connerney et al., 2022). One region which previously showed significant differences between the observed and predicted satellite footprint location is the auroral kink sector, at longitudes from 80° to 150°, for which Grodent et al. (2008) suggested the inclusion of a magnetic anomaly to the existing magnetic field model at that time, in order to better fit the footprint location. Early Juno measurement for instance showed significant differences between the predicted Europa footprint, and the observed one (Allegrini et al., 2020b). JRM33 is now in very good agreement with the observed MAW positions in that sector.

Despite the greater coverage than HST in the south, there are several longitude gaps in the northern MAW observation not covered by Juno-UVS as of PJ43. For the north-

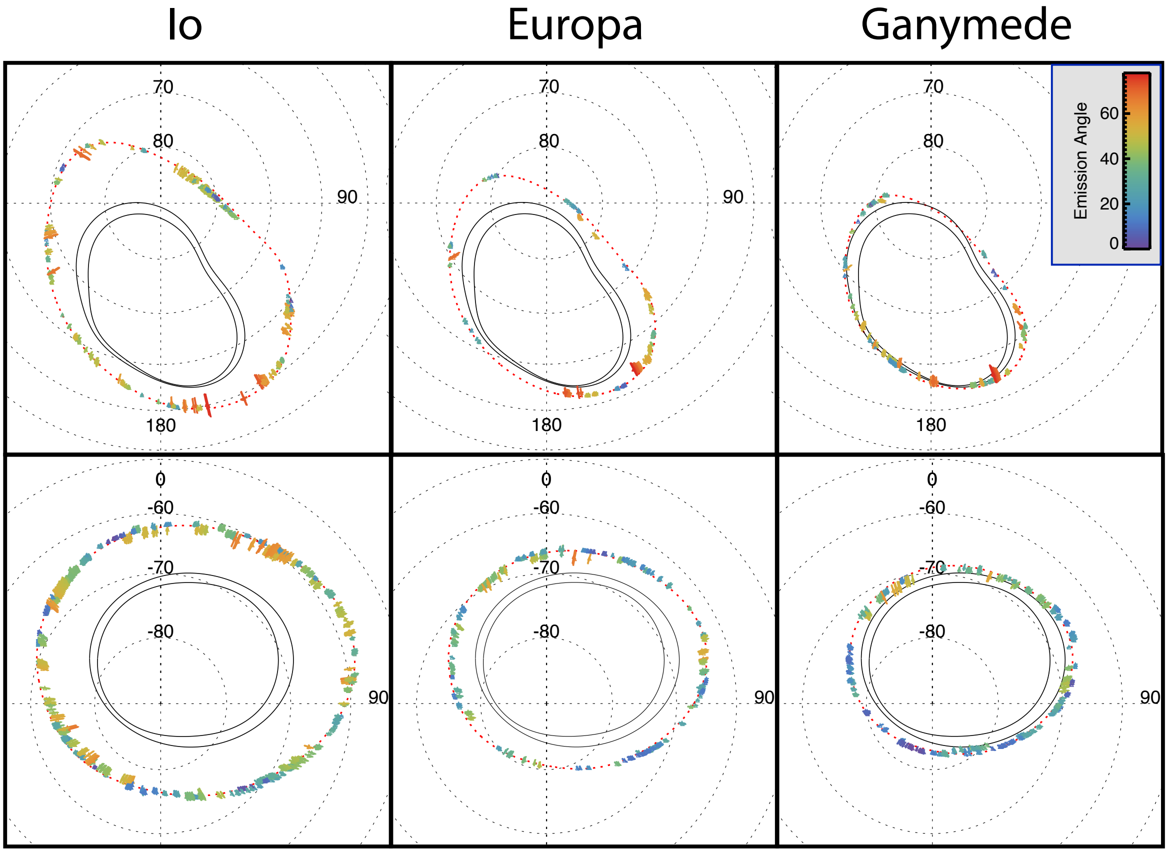

Figure 3. Extracted position of the Io, Europa and Ganymede Main Alfvén Wing footprints in the north (top panels) and south (bottom panels), using Juno-UVS data recorded from perijoves 1 to 43 and color-coded according to the emission angle observed by Juno-UVS. The solid black lines show the reference oval from Bonfond et al. (2012). The red dotted line show the satellite footpaths as predicted from the JRM33 model (Connerney et al., 2022).

ern Io MAW, there remains a gap at footprint longitudinal sectors of 260°-280°; 100°-118°; 342°-20°. For the northern Europa MAW, the gaps are 300°-80°; 175°-206°; 215°-238°; 250°-290°. For the northern Ganymede MAW, the main longitude gap is 280°-130°. The MAW footprint location for Io, Europa and Ganymede are provided in the supporting information. The difference in coverage with previous HST observations can be compared with Figures 1 and 2 showed in the supporting information of Bonfond, Saur, et al. (2017).

By binning the measured MAW positions over 1.5°-wide longitudinal sector, one can assess the accuracy of magnetic field models, such as JRM33. In order to reduce the uncertainty resulting from the viewing geometry, only the MAW position recorded at emission angle lower than 20° were selected. For Io, the average distance between the JRM33-computed footpath and the observed MAW positions is 511 ± 28 km in the north and 274 ± 64 km in the south. For Europa, these numbers are 141 ± 26 km in the north and 322 ± 61 km in the south. For Ganymede, the remaining uncertainties are 213 ± 44 km in the north and 343 ± 64 km in the south. These numbers provide an order or magnitude estimate in mapping precision between the model and the observations, and vary slightly depending on the way the UVS data is binned (*e.g.,* longitudinal and emission angle binning).

The measurement of the MAW position now allows providing an estimate of the equatorial lead angle, when used in combination with a magnetic field model.

4 Lead angles

The equatorial lead angle is the longitudinal difference, in the orbital plane of the moon, between the actual position of the moons and the position of the MAW footprints mapped instantaneously to the orbital plane of the moon. That information contains the sum of the physical processes occurring between the interaction region around the moon and Jupiter's ionosphere, from the propagation of the Alfvén waves through the plasma sheet to its partial reflection and transmission at the plasma density gradients.

The knowledge of the lead angle is crucial for the interpretation of the moon-related decametric emission (e.g., S. L. G. Hess, Pétin, et al., 2010; Marques et al., 2017; Louis et al., 2019; Lamy et al., 2022). Moon-induced radio emission are thought to originate from the cyclotron maser instability (CMI), a wave-particle instability where a circularly polarized wave resonates with the gyrating motion of an accelerated electron population (e.g., Zarka et al., 2018, for review). That mechanism was confirmed using Juno in-situ measurements (Louarn et al., 2017). These radio emissions are emitted along a thing hollow cone around a given magnetic field line, with a cone thickness on the order of a degree, and the beaming angle of these emissions depends on the electron energy (S. Hess et al., 2008). In order to interpret the moon-induced decametric emission, modeling tools such as ExPRES (Louis et al., 2019) require knowledge of both the lead angle and electrons velocity. This may lead to situations were non-unique solutions exist, in order to reproduce the observed decametric radio arcs. The knowledge of the active field line, and thus the leading angle, constitutes one of the main source of uncertainty in determining the electron energy responsible for the radio emission (S. L. G. Hess, Pétin, et al., 2010; Lamy et al., 2022). Previous estimations of the absolute lead angle values were not accurate enough and only the relative lead angle between the secondary spots were trustworthy, mostly because of the uncertainty in the magnetic field models as well as the uncertainties in the Europa and Ganymede measured footprint positions from HST (S. L. G. Hess, Pétin, et al., 2010).

Additionally, Juno in-situ instruments provided invaluable measurements of the particle distribution on the magnetic field lines connected to the satellite footprints and tails, such as measurements connected to Io (Szalay et al., 2018; Clark et al., 2020; Sulaiman et al., 2020; Szalay et al., 2020b), Europa (Allegrini et al., 2020a) and Ganymede (Szalay et al., 2020a; Louis et al., 2020; Hue et al., 2022). Szalay et al. (2020b) showed that the exponential decrease in precipitating electron energy flux, obtained by the Juno-JADE instrument when Juno was connected at various distances downstream the Io footprint tail, was better organized when considering the angular separation along Io's orbit between Io and an Alfvén waves back-traced from Jupiter's ionosphere to the moon equatorial plane. That quantities, coined "Io-Alfvén tail distance" wraps up the knowledge of the equatorial lead angle within.

Figures 4 and 5 display the equatorial lead angle in the north and south, respectively, measured by Juno-UVS and using the JRM33 magnetic field model (Connerney et al., 2022) combined with the Juno-era current sheet model (Connerney et al., 2020), and color-coded according to the perijove it was recorded at. The lead angle depends mainly on the travel distance variation of the Alfvén waves through the region with denser plasma, *i.e.,* the plasma sheet and Jupiter's ionosphere. Assuming an homogeneous plasma sheet with space and time at the first order, one would expect a sinusoidal modulation of that angle with the latitudinal separation between the moons and the center of the plasma sheet over a complete Jovian rotation (S. L. G. Hess, Pétin, et al., 2010). Figures 4 and 5 are fitted with a first order Fourier series, such as:

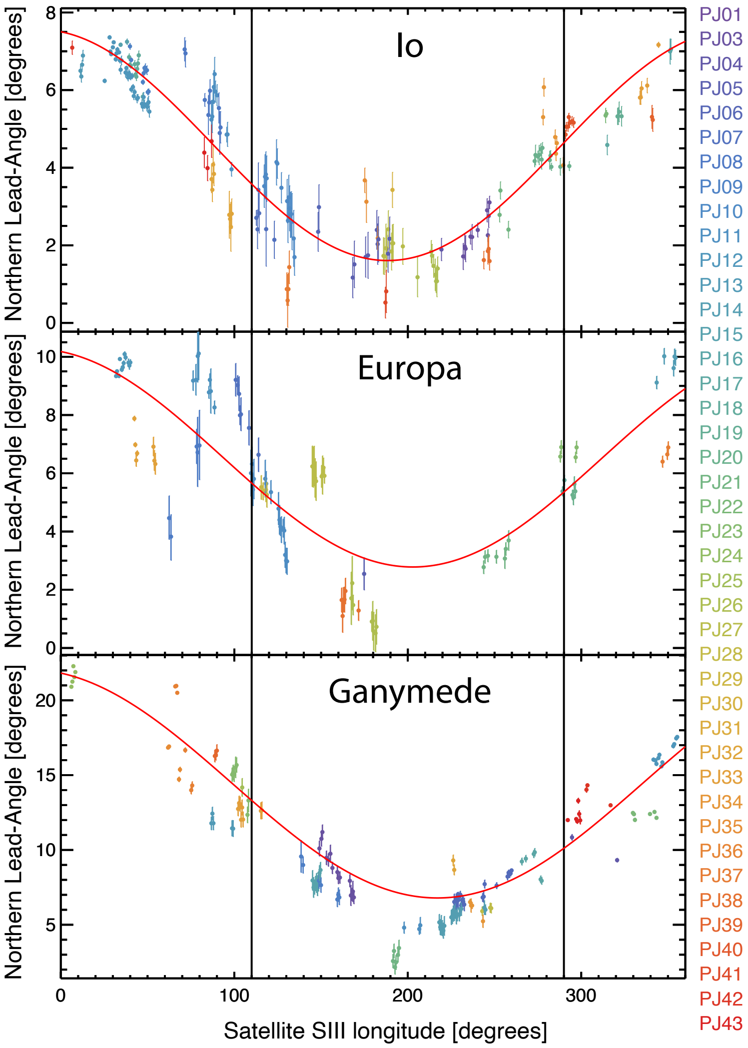

Figure 4. Northern lead angle for Io (top), Europa (middle) and Ganymede (bottom) using Juno-UVS dataset of the Main Alfvén Wing from PJ1 until PJ43. The vertical solid black lines indicate the location when the moons are at the center of the plasma sheet.

$$L = a_0 + a_1 \cos w\lambda_{III} + b_1 \sin w\lambda_{III} \tag{3}$$

The best fit parameters of equation 3 were estimates using the MPFIT package (Markwardt, 2009), and are listed on Table 1. The averaged values of the northern and southern Io lead angles are $4.2^{+0.5}_{-0.6}$ degrees and $4.22^{+0.02}_{-0.04}$ degrees, respectively. For Europa, these values are $5.8^{+1.3}_{-1.7}$ degrees in the north, and $7.01^{+0.03}_{-0.0001}$ degrees in the south. For Ganymede, the averaged northern and southern lead angles are $12.5^{+0.4}_{-0.4}$ degrees and $13.07^{+0.03}_{-0.03}$ degrees, respectively. The uncertainties on the averaged lead angle is calculated using the 3-sigma uncertainties of the derived parameters, and are tighter in the south, due to the denser dataset. The averaged northern and southern lead angles are self-consistent for each individual moon, except for Ganymede whose averaged northern and southern lead angles do not overlap by a slight margin.

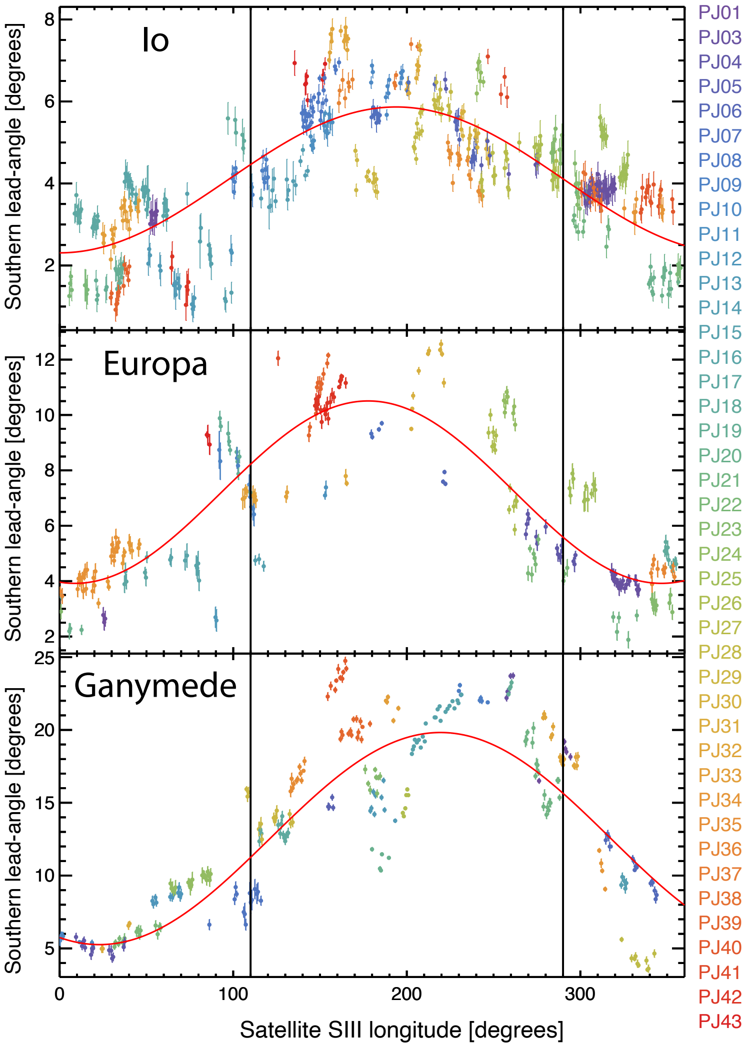

Figure 5. Same as Fig. 4 for the south.

The lead angle shows a considerable variability at a given SIII longitude, well beyond the observational uncertainties. Since this quantity accounts for the sum of the physical processes occurring between the interaction region around the moon and Jupiter's ionosphere, it is affected by changes in the physical condition in the plasma sheet. For Io, Hinton et al. (2019) estimated that the Alfvén travel times to Jupiter's southern ionosphere at $\lambda_{III}^{Io} = 200°$ ranged from 11 min to 13.5 min solely based on torus density variations on the order of 50% caused by variation in Io's volcanic activity (Yoshikawa et al., 2017). Based on Io's synodic period, a 2.5 min variation in Alfvén travel times corresponds to a longitudinal shift of about 1.5°, which is fully consistent with the lead angle variations observed between perijoves. However, Hinton et al. (2019) also predicted a variation in the Alfvén travel times to Jupiter's southern ionosphere at $\lambda_{III}^{Io} = 30°$ from 2 min to 3 min, leading to a predicted shift in lead angle of 0.6°, which appears smaller than the measured variation in lead angle in that longitude sector. The origin of this discrepancy is not clear, and could be due to either underestimating the uncertainties of the lead angle, uncertainties in the magnetic field model or simplification in modeling the plasma sheet spatial variability.

	North	South
Io	L = 4.6 + 2.9 cos 0.9 λ - 0.6 sin 0.9 λ	L = 4.1 - 1.8 cos 0.93 λ - 0.004 sin 0.93 λ
Europa	L = 6.5 + 3.6 cos 0.8 λ - 0.8 sin 0.8 λ	L = 7.2 - 3.2 cos 1.06 λ - 0.5 sin 1.06 λ
Ganymede	L = 14.4 + 7.4 cos 0.76 λ - 1.9 sin 0.76 λ	L = 12.5 - 6.8 cos 0.92 λ - 2.6 sin 0.92 λ

Table 1. Best fit of the northern and southern lead angles for Io, Europa and Ganymede.

The Alfvén travel times can be estimated for each moon using equation (4).

$$t_A = \frac{P^{syn}_{moon} \times \delta_{moon}}{360}, \tag{4}$$

where P^{syn}_{moon} is the synodic period and δ_{moon} the measured lead angle of the considered moon. The range of Alfvén travel times are listed on 2. The derived Io Alfvén travel times are consistent with the modeled travel times by Hinton et al. (2019).

	North	South
Io	t_A^{min} = 3.5 minutes t_A^{max} = 16.1 minutes	t_A^{min} = 4.9 minutes t_A^{max} = 12.7 minutes
Europa	t_A^{min} = 5.2 minutes t_A^{max} = 18.9 minutes	t_A^{min} = 7.4 minutes t_A^{max} = 19.5 minutes
Ganymede	t_A^{min} = 11.9 minutes t_A^{max} = 38.3 minutes	t_A^{min} = 9.2 minutes t_A^{max} = 34.7 minutes

Table 2. Range of northern and southern hemisphere Alfvén travel times for Io, Europa and Ganymede estimated from the measured lead angles.

5 Application to modeling of the moon-induced decametric emission

This section illustrates the added gain from the equatorial lead angle knowledge in interpreting the moon-induced decametric radio emission. Several datasets of such emission were recorded by the Radio and Plasma Wave Science (RPWS) measurements on Cassini (Gurnett et al., 2004) on 17 November 2000, prior to the Jupiter flyby. Figure 6 shows the analysis of a decametric arc induced by Ganymede, and previously studied by Louis et al. (2017).

RPWS data is shown on panels D and E as time-frequency spectrogram, corresponding to a Ganymede-D decametric arc, *i.e.,* emitted on a field line connecting Ganymede and Jupiter southern hemisphere around Jupiter's dawn side. Because the waves amplified by the cyclotron maser instability are circularly polarized, panel D shows the time-frequency spectrogram corresponding to the polar circularization, for better contrast.

Panel A shows the best fit to the data using the ExPRES radio modeling (Louis et al., 2019). This assumes (i) the radio emission is created by a loss-cone electron distribution with energies of 3 keV, (ii) the JRM33 magnetic field model, and (iii) no equatorial lead angle. Although it was previously presented by Louis et al. (2017), this differs slightly from that earlier work which assumed the IsSAC magnetic field model (S. L. G. Hess et al., 2017). Panel B shows simulations using ExPRES considering the equatorial lead

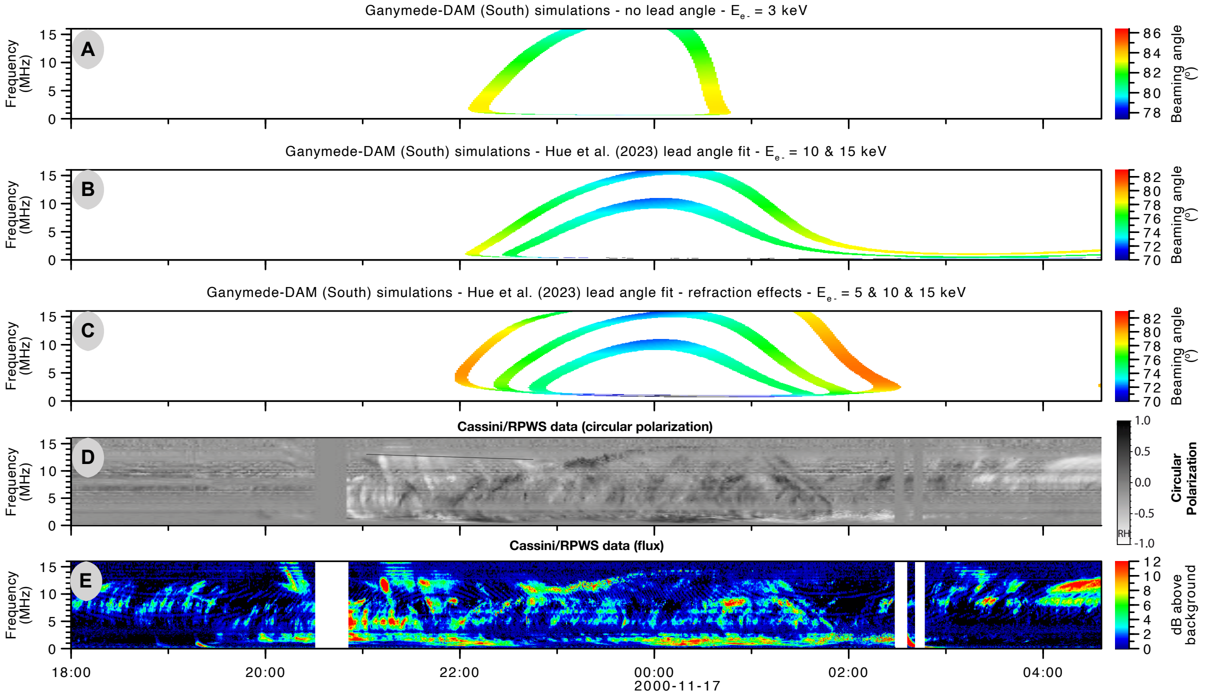

Figure 6. Panel A: ExPRES simulation of a Ganymede-D decametric arc without lead angle. Panel B: ExPRES simulation using the lead angle derived from this present study. Panel C: ExPRES simulation combining the lead angle derived from this present and refraction effect on the emission. Panel D: Cassini-RPWS time-frequency spectrogram of circularly polarized radio emission. Panel E: Cassini-RPWS time-frequency spectrogram.

angle fit derived from the present work. The best fit of the data is obtained considering electrons with energies ranging from 10-15 keV. When accounting for refraction effects on the beamed radio emissions, the fit can be improved by considering electrons of energies ranging 5-15 keV (panel C). Refraction effects are occuring when the radio emissions is emitted in a region with decreasing electron cyclotron frequency (f_{ce}). In which case, the emission can not propagate due to the cut-off frequency at f_{ce}, and the radio wave is reflected until it reaches a region with increasing f_{ce} (Corentin, could you provide some refs here, please?).

The addition of the knowledge of the equatorial angle, especially for Europa and Ganymede, drastically improves the predictability and analysis of moon-induced decametric radio emission. For instance, comparing in more details the simulations that account for the lead angle and refractions effects with the circularly polarized radio emission from RPWS indicate that the early part of the radio emission arc (from 22:00:00 to 22:15:00) are better reproduced with electrons with lower energies, *i.e.,* 3 keV, while the center of the arc is better reproduced with electrons with energies ranging from 10-15 keV. During the Ganymede fluxtube crossing recorded during PJ20 (29 May 2019), Louis et al. (2020) inferred that the large radio emission amplification was caused by electrons with energies ranging from 4-15 keV, in agreement with the ExPRES modeling of the RPWS data.

6 Discussion and Summary

The presented work make use of 479 and 1148 individual spectral images of the satellite footprints recorded over the northern and southern auroral regions, respectively, recorded by Juno-UVS over the first forty-third perijoves. Additional UVS data are available, though were recorded at further distance from the planet, therefore at a lower spatial resolution. From these images, the accurate positions of the Io, Europa and Ganymede Main Alfvén Wing spots are derived and compared with the prediction from the magnetic field model obtained at the end of Juno's prime mission, JRM33 (Connerney et al., 2022). By restricting to data recorded with emission angles lower than 20°, the accuracy with predictions from JRM33 is estimated while limiting the projection effect. The average distance between the JRM33-computed moon footpaths and the observed MAW positions are generally around 500 km or below.

Measurements of the equatorial lead angle provide information about the how the Alfvén waves generated around the moon interaction region propagate until the Jovian ionosphere. It is an important information for analyzing the satellite-induced decametric radio emission as well as interpreting the auroral footprint related in-situ measurements made by Juno. Despite the variability in the measured lead angle at a given moon longitude, a statistically consistent trend can be derived from the first forty-third perijoves. That variability is likely due to temporal and spatial variations of the plasma sheet. The best fit of the lead angle for Io ranges from 1.6°-7.5°, with an overall average of 4.2°. For Europa, the lead angle ranges from 2.8°-10.4°, with an overall average of 6.4°. For Ganymede, the lead angle ranges from 5.3°-21.8°, with an overall average of 12.7°. Over an entire Jovian rotation, this corresponds to Alfvén travel times ranging from 3.5-16.1 minutes, 5.2-19.5 minutes, and 9.2-38.3 minutes for Io, Europa and Ganymede, respectively.

Modeling the moon-induced decametric arc requires the knowledge of the equatorial lead angle to constrain with higher accuracy the derived electron energy causing the emission. The equatorial lead angle values fit from this work brings the derived electron energy required to reproduce the Ganymede-induced decametric arc closer to the in-situ measured value from Juno. This method can be applied for modeling moon-induced radio emission for which no in-situ data is available.

The main conclusions of this work are listed hereafter.

1. The reported position of the Main Alfvén wing spots for Io, Europa and Ganymede agrees well with the JRM33-computed satellite footpath within 500 km as mapped on Jupiter.
2. The averaged equatorial lead angle for Io, Europa and Ganymede is measured to be 4.2°, 6.4°, and 12.7°, respectively.
3. The range of Alfvén travel times for Io, Europa and Ganymede are 3.5-16.1 minutes, 5.2-19.5 minutes, and 9.2-38.3 minutes, respectively.
4. Empirical formulae for the Io, Europa and Ganymede lead angles derived from Juno data are provided.
5. Including the knowledge of the equatorial lead angle in modeling the moon-induced decametric emission allows deriving electron energies causing the emissions in agreement with Juno in-situ measurements.

Acknowledgments

We are grateful to NASA and contributing institutions that have made the Juno mission possible. This work was funded by the NASA New Frontiers Program for Juno (managed by the Jet Propulsion Laboratory) via a subcontract with Southwest Research Institute. BB, JCG and DG acknowledge funding for this research by a PRODEX contract of ESA, managed with the help of BELSPO. The work of MI was supported by the

JSPS KAKENHI Grant Number JP20K22371. All the data used in this study are publicly available on the PDS Atmospheres Node Data Set Catalog `https://pds-atmospheres.nmsu.edu/data_and_services/atmospheres_data/JUNO/juno.html`.

References

Acton, C., Bachman, N., Semenov, B., & Wright, E. (2018, January). A look towards the future in the handling of space science mission geometry. , *150*, 9-12. doi: 10.1016/j.pss.2017.02.013

Acton, C. H. (1996, January). Ancillary data services of NASA's Navigation and Ancillary Information Facility. , *44*(1), 65-70. doi: 10.1016/0032-0633(95)00107-7

Allegrini, F., Gladstone, G. R., Hue, V., Clark, G., Szalay, J. R., Kurth, W. S., … Wilson, R. J. (2020a, September). First Report of Electron Measurements During a Europa Footprint Tail Crossing by Juno. , *47*(18), e89732. doi: 10.1029/2020GL089732

Allegrini, F., Gladstone, G. R., Hue, V., Clark, G., Szalay, J. R., Kurth, W. S., … Wilson, R. J. (2020b, September). First Report of Electron Measurements During a Europa Footprint Tail Crossing by Juno. , *47*(18), e89732. doi: 10.1029/2020GL089732

Bagenal, F., Adriani, A., Allegrini, F., Bolton, S. J., Bonfond, B., Bunce, E. J., … Zarka, P. (2017, November). Magnetospheric Science Objectives of the Juno Mission. , *213*(1-4), 219-287. doi: 10.1007/s11214-014-0036-8

Bagenal, F., & Dols, V. (2020, May). The Space Environment of Io and Europa. *Journal of Geophysical Research (Space Physics)*, *125*(5), e27485. doi: 10.1029/2019JA027485

Bigg, E. K. (1964, September). Influence of the Satellite Io on Jupiter's Decametric Emission. *Nature*, *203*, 1008-1010. doi: 10.1038/2031008a0

Bolton, S. J., Adriani, A., Adumitroaie, V., Allison, M., Anderson, J., Atreya, S., … Wilson, R. (2017, May). Jupiter's interior and deep atmosphere: The initial pole-to-pole passes with the Juno spacecraft. *Science*, *356*, 821-825. doi: 10.1126/science.aal2108

Bonfond, B. (2010, September). The 3-D extent of the Io UV footprint on Jupiter. *Journal of Geophysical Research (Space Physics)*, *115*(A9), A09217. doi: 10.1029/2010JA015475

Bonfond, B., Gladstone, G. R., Grodent, D., Gérard, J. C., Greathouse, T. K., Hue, V., … Connerney, J. E. P. (2018, Nov). Bar Code Events in the Juno-UVS Data: Signature 10 MeV Electron Microbursts at Jupiter. , *45*(22), 12,108-12,115. doi: 10.1029/2018GL080490

Bonfond, B., Gladstone, G. R., Grodent, D., Greathouse, T. K., Versteeg, M. H., Hue, V., … Kurth, W. S. (2017, May). Morphology of the UV aurorae Jupiter during Juno's first perijove observations. , *44*, 4463-4471. doi: 10.1002/2017GL073114

Bonfond, B., Grodent, D., Gérard, J.-C., Radioti, A., Saur, J., & Jacobsen, S. (2008, March). UV Io footprint leading spot: A key feature for understanding the UV Io footprint multiplicity? *Geophys. Res. Lett.*, *35*, L05107. doi: 10.1029/2007GL032418

Bonfond, B., Grodent, D., Gérard, J. C., Stallard, T., Clarke, J. T., Yoneda, M., … Gustin, J. (2012, January). Auroral evidence of Io's control over the magnetosphere of Jupiter. , *39*(1), L01105. doi: 10.1029/2011GL050253

Bonfond, B., Saur, J., Grodent, D., Badman, S. V., Bisikalo, D., Shematovich, V., … Radioti, A. (2017, August). The tails of the satellite auroral footprints at Jupiter. *Journal of Geophysical Research (Space Physics)*, *122*, 7985-7996. doi: 10.1002/2017JA024370

Bonfond, B., Yao, Z. H., Gladstone, G. R., Grodent, D., Gérard, J. C., Matar, J., …

Bolton, S. J. (2021, March). Are Dawn Storms Jupiter's Auroral Substorms? *AGU Advances*, *2*(1), e00275. doi: 10.1029/2020AV000275

Clark, G., Mauk, B. H., Kollmann, P., Szalay, J. R., Sulaiman, A. H., Gershman, D. J., … Westlake, J. (2020, December). Energetic Proton Acceleration Associated With Io's Footprint Tail. , *47*(24), e90839. doi: 10.1029/2020GL090839

Clarke, J. T., Ajello, J., Ballester, G., Ben Jaffel, L., Connerney, J., Gérard, J.-C., … Waite, J. H. (2002, February). Ultraviolet emissions from the magnetic footprints of Io, Ganymede and Europa on Jupiter. , *415*, 997-1000.

Clarke, J. T., Ballester, G. E., Trauger, J., Evans, R., Connerney, J. E. P., Stapelfeldt, K., … Westphal, J. A. (1996, October). Far-Ultraviolet Imaging of Jupiter's Aurora and the lo "Footprint". *Science*, *274*, 404-409. doi: 10.1126/science.274.5286.404

Connerney, J. E. P., Acuña, M. H., Ness, N. F., & Satoh, T. (1998, June). New models of Jupiter's magnetic field constrained by the Io flux tube footprint. , *103*, 11929-11940. doi: 10.1029/97JA03726

Connerney, J. E. P., Adriani, A., Allegrini, F., Bagenal, F., Bolton, S. J., Bonfond, B., … Waite, J. (2017, May). Jupiter's magnetosphere and aurorae observed by the Juno spacecraft during its first polar orbits. *Science*, *356*, 826-832. doi: 10.1126/science.aam5928

Connerney, J. E. P., Baron, R., Satoh, T., & Owen, T. (1993, November). Images of Excited H_3ˆ+ at the Foot of the Io Flux Tube in Jupiter's Atmosphere. *Science*, *262*, 1035-1038. doi: 10.1126/science.262.5136.1035

Connerney, J. E. P., Timmins, S., Herceg, M., & Joergensen, J. L. (2020, October). A Jovian Magnetodisc Model for the Juno Era. *Journal of Geophysical Research (Space Physics)*, *125*(10), e28138. doi: 10.1029/2020JA028138

Connerney, J. E. P., Timmins, S., Oliversen, R. J., Espley, J. R., Joergensen, J. L., Kotsiaros, S., … Levin, S. M. (2022, February). A New Model of Jupiter's Magnetic Field at the Completion of Juno's Prime Mission. *Journal of Geophysical Research (Planets)*, *127*(2), e07055. doi: 10.1029/2021JE007055

Damiano, P. A., Delamere, P. A., Stauffer, B., Ng, C. S., & Johnson, J. R. (2019, March). Kinetic Simulations of Electron Acceleration by Dispersive Scale Alfvén Waves in Jupiter's Magnetosphere. , *46*(6), 3043-3051. doi: 10.1029/2018GL081219

Davis, M. W., Gladstone, G. R., Greathouse, T. K., Slater, D. C., Versteeg, M. H., Persson, K. B., … Eterno, J. S. (2011). Radiometric performance results of the Juno ultraviolet spectrograph (Juno-UVS). In (Vol. 8146, p. 814604). doi: 10.1117/12.894274

Delamere, P. A., Bagenal, F., Ergun, R., & Su, Y. J. (2003, June). Momentum transfer between the Io plasma wake and Jupiter's ionosphere. *Journal of Geophysical Research (Space Physics)*, *108*(A6), 1241. doi: 10.1029/2002JA009530

Ebert, R. W., Greathouse, T. K., Clark, G., Hue, V., Allegrini, F., Bagenal, F., … Wilson, R. J. (2021, December). Simultaneous UV Images and High-Latitude Particle and Field Measurements During an Auroral Dawn Storm at Jupiter. *Journal of Geophysical Research (Space Physics)*, *126*(12), e29679. doi: 10.1029/2021JA029679

Gérard, J.-C., Saglam, A., Grodent, D., & Clarke, J. T. (2006, April). Morphology of the ultraviolet Io footprint emission and its control by Io's location. *Journal of Geophysical Research (Space Physics)*, *111*, A04202. doi: 10.1029/2005JA011327

Gershman, D. J., Connerney, J. E. P., Kotsiaros, S., DiBraccio, G. A., Martos, Y. M., -Viñas, A. F., … Bolton, S. J. (2019, July). Alfvénic Fluctuations Associated With Jupiter's Auroral Emissions. , *46*(13), 7157-7165. doi: 10.1029/2019GL082951

Gladstone, G. R., Persyn, S. C., Eterno, J. S., Walther, B. C., Slater, D. C., Davis,

M. W., … Denis, F. (2017, November). The Ultraviolet Spectrograph on NASA's Juno Mission. , *213*, 447-473. doi: 10.1007/s11214-014-0040-z

Greathouse, T. K., Gladstone, G. R., Davis, M. W., Slater, D. C., Versteeg, M. H., Persson, K. B., … Eterno, J. S. (2013, September). Performance results from in-flight commissioning of the Juno Ultraviolet Spectrograph (Juno-UVS). In *Uv, x-ray, and gamma-ray space instrumentation for astronomy xviii* (Vol. 8859, p. 88590T). doi: 10.1117/12.2024537

Grodent, D., Bonfond, B., GéRard, J.-C., Radioti, A., Gustin, J., Clarke, J. T., … Connerney, J. E. P. (2008, September). Auroral evidence of a localized magnetic anomaly in Jupiter's northern hemisphere. *Journal of Geophysical Research (Space Physics)*, *113*(A9), A09201. doi: 10.1029/2008JA013185

Gurnett, D. A., & Goertz, C. K. (1981, February). Multiple Alfven wave reflections excited by Io: origin of the Jovian decametric arcs. , *86*(A2), 717-722. doi: 10.1029/JA086iA02p00717

Gurnett, D. A., Kurth, W. S., Kirchner, D. L., Hospodarsky, G. B., Averkamp, T. F., Zarka, P., … Pedersen, A. (2004, September). The Cassini Radio and Plasma Wave Investigation. , *114*(1-4), 395-463. doi: 10.1007/s11214-004-1434-0

Hess, S., Cecconi, B., & Zarka, P. (2008, July). Modeling of Io-Jupiter decameter arcs, emission beaming and energy source. , *35*(13), L13107. doi: 10.1029/2008GL033656

Hess, S. L. G., Bonfond, B., Bagenal, F., & Lamy, L. (2017, January). A model of the Jovian internal field derived from in-situ and auroral constraints. In G. Fischer, G. Mann, M. Panchenko, & P. Zarka (Eds.), *Planetary radio emissions viii* (p. 157-167). doi: 10.1553/PRE8s157

Hess, S. L. G., Bonfond, B., Zarka, P., & Grodent, D. (2011, May). Model of the Jovian magnetic field topology constrained by the Io auroral emissions. *Journal of Geophysical Research (Space Physics)*, *116*, A05217. doi: 10.1029/2010JA016262

Hess, S. L. G., Delamere, P., Dols, V., Bonfond, B., & Swift, D. (2010, June). Power transmission and particle acceleration along the Io flux tube. *Journal of Geophysical Research (Space Physics)*, *115*, A06205. doi: 10.1029/2009JA014928

Hess, S. L. G., Pétin, A., Zarka, P., Bonfond, B., & Cecconi, B. (2010, August). Lead angles and emitting electron energies of Io-controlled decameter radio arcs. , *58*(10), 1188-1198. doi: 10.1016/j.pss.2010.04.011

Hinton, P. C., Bagenal, F., & Bonfond, B. (2019). Alfvén wave propagation in the io plasma torus. *Geophysical Research Letters*, *46*(3), 1242-1249. Retrieved from `https://agupubs.onlinelibrary.wiley.com/doi/abs/10.1029/2018GL081472` doi: 10.1029/2018GL081472

Hue, V., Giles, R. S., Gladstone, G. R., Greathouse, T. K., Davis, M. W., Kammer, J. A., & Versteeg, M. H. (2021, October). Updated radiometric and wavelength calibration of the Juno ultraviolet spectrograph. *Journal of Astronomical Telescopes, Instruments, and Systems*, *7*, 044003. doi: 10.1117/1.JATIS.7.4.044003

Hue, V., Gladstone, G. R., Greathouse, T. K., Kammer, J. A., Davis, M. W., Bonfond, B., … Byron, B. D. (2019, Feb). In-flight Characterization and Calibration of the Juno-ultraviolet Spectrograph (Juno-UVS). , *157*(2), 90. doi: 10.3847/1538-3881/aafb36

Hue, V., Greathouse, T. K., Bonfond, B., Saur, J., Gladstone, G. R., Roth, L., … Bagenal, F. (2019, July). Juno-UVS Observation of the Io Footprint During Solar Eclipse. *Journal of Geophysical Research (Space Physics)*, *124*(7), 5184-5199. doi: 10.1029/2018JA026431

Hue, V., Szalay, J. R., Greathouse, T. K., Bonfond, B., Kotsiaros, S., Louis, C. K., … Mauk, B. H. (2022, April). A Comprehensive Set of Juno In Situ and Remote Sensing Observations of the Ganymede Auroral Footprint. , *49*(7), e96994. doi: 10.1029/2021GL096994

Kammer, J. A., Hue, V., Greathouse, T. K., Gladstone, G. R., Davis, M. W., & Versteeg, M. H. (2019, April). Planning operations in Jupiter's high-radiation environment: optimization strategies from Juno-ultraviolet spectrograph. *Journal of Astronomical Telescopes, Instruments, and Systems*, *5*, 027001. doi: 10.1117/1.JATIS.5.2.027001

Lamy, L., Colomban, L., Zarka, P., Prangé, R., Marques, M. S., Louis, C. K., ... Yerin, S. (2022, April). Determining the Beaming of Io Decametric Emissions: A Remote Diagnostic to Probe the Io-Jupiter Interaction. *Journal of Geophysical Research (Space Physics)*, *127*(4), e30160. doi: 10.1029/2021JA030160

Louarn, P., Allegrini, F., McComas, D. J., Valek, P. W., Kurth, W. S., André, N., ... Zink, J. L. (2017, May). Generation of the Jovian hectometric radiation: First lessons from Juno. , *44*(10), 4439-4446. doi: 10.1002/2017GL072923

Louarn, P., Allegrini, F., McComas, D. J., Valek, P. W., Kurth, W. S., André, N., ... Wilson, R. J. (2018, September). Observation of Electron Conics by Juno: Implications for Radio Generation and Acceleration Processes. , *45*(18), 9408-9416. doi: 10.1029/2018GL078973

Louis, C. K., Hess, S. L. G., Cecconi, B., Zarka, P., Lamy, L., Aicardi, S., & Loh, A. (2019, July). ExPRES: an Exoplanetary and Planetary Radio Emissions Simulator. , *627*, A30. doi: 10.1051/0004-6361/201935161

Louis, C. K., Lamy, L., Zarka, P., Cecconi, B., & Hess, S. L. G. (2017, September). Detection of Jupiter decametric emissions controlled by Europa and Ganymede with Voyager/PRA and Cassini/RPWS. *Journal of Geophysical Research (Space Physics)*, *122*(9), 9228-9247. doi: 10.1002/2016JA023779

Louis, C. K., Louarn, P., Allegrini, F., Kurth, W. S., & Szalay, J. R. (2020, October). Ganymede-Induced Decametric Radio Emission: In Situ Observations and Measurements by Juno. , *47*(20), e90021. doi: 10.1029/2020GL090021

Markwardt, C. B. (2009, September). Non-linear Least-squares Fitting in IDL with MPFIT. In D. A. Bohlender, D. Durand, & P. Dowler (Eds.), *Astronomical data analysis software and systems xviii* (Vol. 411, p. 251).

Marques, M. S., Zarka, P., Echer, E., Ryabov, V. B., Alves, M. V., Denis, L., & Coffre, A. (2017, August). Statistical analysis of 26 yr of observations of decametric radio emissions from Jupiter. , *604*, A17. doi: 10.1051/0004-6361/201630025

Mura, A., Adriani, A., Connerney, J. E. P., Bolton, S., Altieri, F., Bagenal, F., ... Turrini, D. (2018, August). Juno observations of spot structures and a split tail in Io-induced aurorae on Jupiter. *Science*, *361*, 774-777. doi: 10.1126/science.aat1450

Neubauer, F. M. (1980, March). Nonlinear standing Alfven wave current system at Io - Theory. *J. Geophys. Res.*, *85*, 1171-1178. doi: 10.1029/JA085iA03p01171

Sulaiman, A. H., Hospodarsky, G. B., Elliott, S. S., Kurth, W. S., Gurnett, D. A., Imai, M., ... Bolton, S. J. (2020, November). Wave-Particle Interactions Associated With Io's Auroral Footprint: Evidence of Alfvén, Ion Cyclotron, and Whistler Modes. , *47*(22), e88432. doi: 10.1029/2020GL088432

Szalay, J. R., Allegrini, F., Bagenal, F., Bolton, S. J., Bonfond, B., Clark, G., ... Wilson, R. J. (2020a, February). Alfvénic Acceleration Sustains Ganymede's Footprint Tail Aurora. , *47*(3), e86527. doi: 10.1029/2019GL086527

Szalay, J. R., Allegrini, F., Bagenal, F., Bolton, S. J., Bonfond, B., Clark, G., ... Wilson, R. J. (2020b, September). A New Framework to Explain Changes in Io's Footprint Tail Electron Fluxes. , *47*(18), e89267. doi: 10.1029/2020GL089267

Szalay, J. R., Bonfond, B., Allegrini, F., Bagenal, F., Bolton, S., Clark, G., ... Wilson, R. J. (2018). In situ observations connected to the io footprint tail aurora. *Journal of Geophysical Research: Planets*, *123*(11), 3061-3077. doi: 10.1029/2018JE005752

Thomas, N., Bagenal, F., Hill, T. W., & Wilson, J. K. (2004). The Io neutral clouds and plasma torus. In F. Bagenal, T. E. Dowling, & W. B. McKinnon (Eds.), *Jupiter. the planet, satellites and magnetosphere* (p. 561-591).

Yoshikawa, I., Suzuki, F., Hikida, R., Yoshioka, K., Murakami, G., Tsuchiya, F., … Fujimoto, M. (2017, August). Volcanic activity on Io and its influence on the dynamics of the Jovian magnetosphere observed by EXCEED/Hisaki in 2015. *Earth, Planets and Space*, *69*(1), 110. doi: 10.1186/s40623-017-0700-9

Zarka, P., Marques, M. S., Louis, C., Ryabov, V. B., Lamy, L., Echer, E., & Cecconi, B. (2018, October). Jupiter radio emission induced by Ganymede and consequences for the radio detection of exoplanets. , *618*, A84. doi: 10.1051/0004-6361/201833586